

## **Catalytic performance of Ni supported apatite-type lanthanum silicates Ni/ATLS-(Ni/La<sub>9.83</sub>Si<sub>4.5</sub>Fe<sub>1.5</sub>O<sub>26±δ</sub>) in glycerol steam reforming reaction**

**P.K. Pandis<sup>1</sup>, N.D. Charisiou<sup>2</sup>, M.A. Goula<sup>2</sup>, V.N. Stathopoulos<sup>1\*</sup>**

<sup>1</sup>*Laboratory of Chemistry and Materials Technology, Department of Electrical Engineering, School of Technological Applications, Technological Educational Institute of Sterea Ellada, Chalkida, 34400 Psachna, Greece*

<sup>2</sup>*Laboratory of Alternative Fuels and Environmental Catalysis, Department of Environmental and Pollution Control Engineering, School of Technological Applications, Technological Educational Institute of Western Macedonia, Koila, 50100, Kozani, Greece*

\*E-mail: [vasta@teihal.gr](mailto:vasta@teihal.gr); [vasta@teiste.gr](mailto:vasta@teiste.gr); Tel: +30 2228099688; +30 2228099621

### **INTRODUCTION**

The disposal of crude glycerol as a by-product of the biodiesel industry is one of the major issues concerning its utilization towards the production for renewable oxygen [1]. Among the various methods of such utilization, the Glycerol Steam Reforming (GSR) reaction has been investigated over various metal supported catalysts with Ru, Rh, Pt, Ni, Co and Fe to be active. In addition, Ni appears as the most promising active metal [2], due to its low cost, its ability towards O–H, C–H and C–C dissociation even more effectively than noble metals [3,4]. On the other hand, apatite type lanthanum silicate (ATLS) materials, as solid oxide electrolytes [5], have interesting redox properties, high oxygen mobility mainly through interstitial oxygen mobility. However only scarce data is yet available on their catalytic properties although promising [6,7]. In this work we report for the first time an ATLS as Ni support in the GSR reaction with promising performance in comparison with alumina supports [8].

### **EXPERIMENTAL**

La<sub>9.83</sub>Si<sub>4.5</sub>Fe<sub>1.5</sub>O<sub>26±δ</sub> (LFSO) sample was prepared by solid state reaction [9,10]. Stoichiometric amounts of metal oxides were mixed, grinded and annealed at 1000°C for 2h with a heating and cooling rate of 3K·min<sup>-1</sup>. Subsequently, the powder was mechanically milled, uniaxially pressed at 18MPa into pellets and sintered at 1500°C. Pellets were crashed, milled to the final material. This powder was agglomerated by uniaxial pressing to form catalytic pellets by a thermal treatment at 1400 °C. Finally, the agglomerated sample was crashed and sieved into the desired fraction between -425µm and +350µm. The as prepared LFSO catalytic support particles had a porosity of 26% as measured by Archimedes method. Commercial γ-Al<sub>2</sub>O<sub>3</sub> (Akzo) was also used as a Ni catalyst support for comparison reasons. The Ni-LFSO and Ni-Al<sub>2</sub>O<sub>3</sub> (Ni-ALO) catalyst was prepared by the wet impregnation method on the supports using Ni(NO<sub>3</sub>)<sub>2</sub>·6H<sub>2</sub>O aqueous solutions to a final loading of 5%wt Ni. Subsequently, they were air-dried overnight and calcined at 800°C/4h. Reduced samples (Ni-LFSOr and Ni-ALOr– r: reduced) were produced under 100ml/min of pure H<sub>2</sub> flow for 1h at 800°C. Ni loading was determined, by ICP-OES (Inductively Coupled Plasma – Optical Emission Spectrometer) by Perkin Elmer (Optima 4300 Dual View model). Typical sample preparation procedure was used as described elsewhere [3,4]. Ni-LFSO, Ni-ALO and LFSO were observed by means of Scanning Electron Microscopy (SEM) using a JEOL6380LV unit. The specific surface area (m<sup>2</sup>/g) was determined by N<sub>2</sub> porosimetry at 77 K using a FISONS SORPTOMATIC 1900 volumetric adsorption/desorption apparatus. Fresh and reduced catalysts were characterized by means of XRD on a SIEMENS D5000 Diffractometer using CuKα radiation (λ = 1.5406 Å) and 2θ range from 10° to 75° with scan step of 0.01°. The Scherrer equation, where applicable, was employed to determine the particle size of different phases based on their most intense diffraction peaks. Thermogravimetric (TGA) and differential thermal analysis (DTA) were performed by a SETARAM TGA 92 system in air environment from 25°C to 900°C with a 10K min<sup>-1</sup> rate at fresh and used catalyst samples in order to investigate carbon accumulation (coking). Catalytic reaction was studied in a stainless steel fixed bed reactor under atmospheric pressure at temperature ranging from 400-750°C in order to investigate the effect of the reaction temperature on (i) glycerol conversion, (ii) glycerol conversion into gaseous products, (iii) hydrogen yield and selectivity, (iv) H<sub>2</sub>/CO molar ratio, and (v) gas and liquid products selectivity or concentration of the produced gas

mixtures at the outlet of the reactor. The experimental set up used allowed the feeding of both liquid and gaseous streams, Prior to catalytic testing, 200 mg of undiluted catalyst (the catalyst bed was supported by quartz wool) was reduced in situ under a flow of 100 v/v % hydrogen ( $100 \text{ ml} \cdot \text{min}^{-1}$ ) at  $800 \text{ }^\circ\text{C}$  for 1 h. The catalyst was then purged with helium for 45 min, the temperature was lowered to  $750 \text{ }^\circ\text{C}$  and the reaction feed was introduced into the catalyst bed. In order to ensure operation at steady state conditions, the catalyst was left for approximately 50 minutes at each step. Liquid products were obtained at the end of this 50 min period.

The reaction feed consisted of the liquid stream - an aqueous solution of 20:80 wt. %  $\text{C}_3\text{H}_8\text{O}_3$  and  $\text{H}_2\text{O}$  (20:1 steam/glycerol molar ratio), with a total liquid flow rate of  $0.12 \text{ ml} \cdot \text{min}^{-1}$  which was kept under continuous stirring at room temperature - and the gas stream (Helium 5.0,  $38 \text{ ml} \cdot \text{min}^{-1}$ ). The glycerol used had 99.5% purity and was obtained from Sigma Aldrich. The gas feed at the reactor's inlet consisted of a gas mixture of 73%  $\text{H}_2\text{O}$ , 4% glycerol and 23% He, corresponding to a WHSV of  $50,000 \text{ ml} \cdot \text{g}^{-1} \cdot \text{h}^{-1}$ .

## RESULTS AND DISCUSSION

From XRD measurements, LFSO and Ni- LFSO materials has been proved stable as no solid state reaction was observed between apatite and NiO or Ni phases (Figure 1a). On the other hand, nickel aluminate crystal phase ( $\text{NiAl}_2\text{O}_4$ ) was detected for the Ni-ALO catalyst. Especially after the reduction of the catalyst, decreased intensities of  $\text{Al}_2\text{O}_3$  and  $\text{NiAl}_2\text{O}_4$  peaks and detection of the  $\text{Ni}^0$  peaks was observed in Ni-ALO catalyst (Figure 1b).

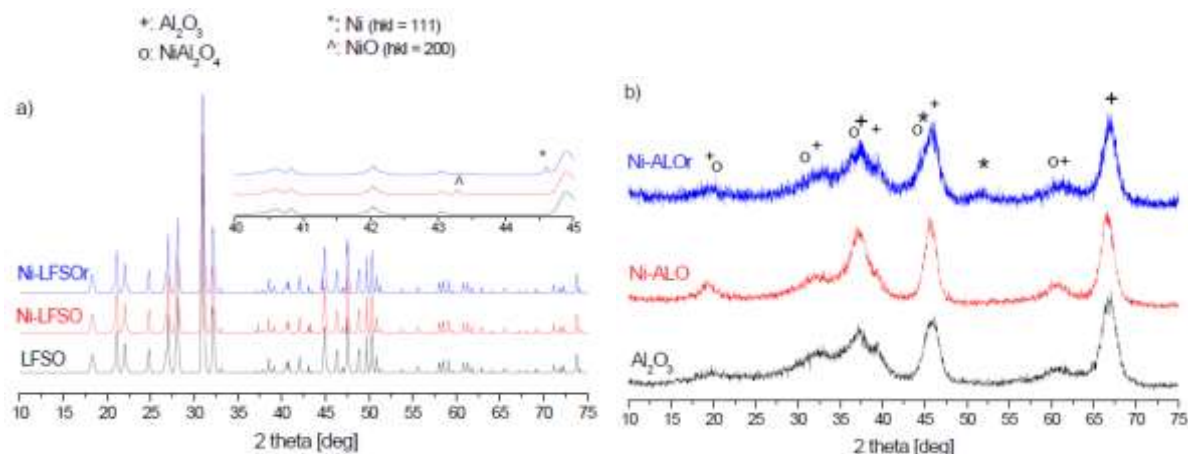


**Figure 1.** XRD for a) LFSO, Ni-LFSO (fresh & reduced catalysts), b)  $\text{Al}_2\text{O}_3$ , Ni-ALO (fresh & reduced catalysts)

For Ni-ALO catalyst glycerol total conversion values showed an increase from 79% at  $400 \text{ }^\circ\text{C}$  to 90% at  $750 \text{ }^\circ\text{C}$  whilst LFSO conversion varies from 80% at  $400 \text{ }^\circ\text{C}$  to 93% at  $750 \text{ }^\circ\text{C}$ . With the incorporation of Ni into LFSO, a rise of conversion values is observed to 86–94% respectively (Fig. 1a left). Ni-LFSO catalyst shows a superior hydrogen selectivity ( $\text{SH}_2$ ) that slightly increases with temperature (Fig. 1b left). Values range from 53.6% ( $400 \text{ }^\circ\text{C}$ ) to 69% ( $750 \text{ }^\circ\text{C}$ ). Up to  $500 \text{ }^\circ\text{C}$  are found to be 3.2 to 1.7 times higher than Ni-ALO. In the whole reaction temperature range, the apatite supported catalytic sample revealed significantly higher hydrogen production compared to the alumina one

Ni-LFSO exhibited a  $\text{H}_2/\text{CO}$  molar ratio ranged from 3 to 5 (Figure 1a right), with its highest value remaining almost stable for temperatures between 450 and  $550 \text{ }^\circ\text{C}$ . On the contrary, for the Ni-ALO sample the  $\text{H}_2/\text{CO}$  molar ratio takes values from 1 to 2 for the same temperature range. The high  $\text{H}_2:\text{CO}$  ratio indicates that the WGS reaction ( $\text{CO} + \text{H}_2\text{O}/\text{H}_2 + \text{CO}_2$ ) is significantly favored in the case of the Ni-LFSO catalyst (Figure 1b right).

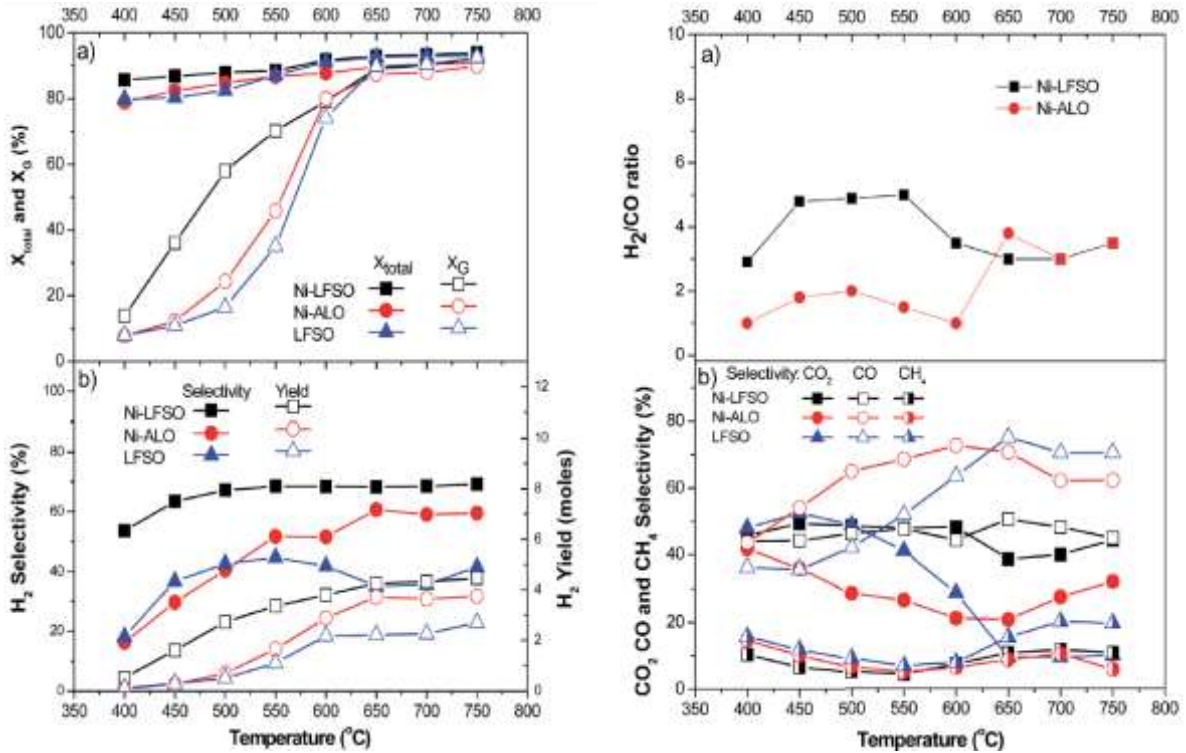


**Figure 2.** (Left: a) Total glycerol conversions and glycerol conversions of gaseous products vs temperature, b)  $H_2$  selectivity and yield vs temperature - Right: a)  $H_2$  to  $CO$  ratio of catalysts, b)  $CO_2$ ,  $CO$  and  $CH_4$  selectivities of Ni-LFSO, Ni-ALO and LFSO vs temperature

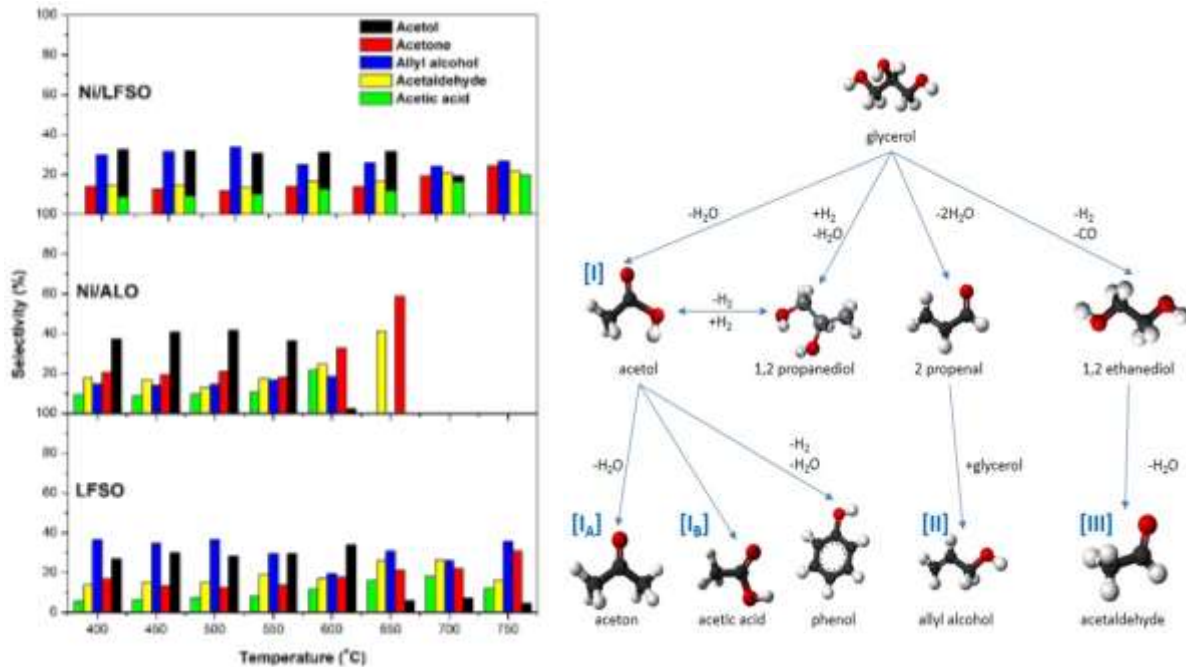


**Figure 3.** Left: Liquid products' selectivities of Ni-LFSO, Ni-ALO and LFSO samples versus temperature – Right: Reaction pathways of liquid products of glycerol

Considering the liquid fraction results (Fig. 3) and the reaction pathways of liquid products of the GSR, the following are observed:

- Ni-ALO catalyst main liquid products were: (i) acetol for  $T < 600$  °C with a maximum value of 45% at 500 °C, (ii) acetone with selectivity values ranging from 20 (400 °C) to 70% (650 °C) and (iii) allyl alcohol, acetaldehyde and acetic acid with quite constant values at 10–15% for temperatures lower than 650 °C. No condensates were detected for reaction temperatures higher than 650 °C.
- Ni-LFSO catalyst liquid products: (i) acetol with a rather constant selectivity value of 30% up to 600 °C and a decreasing trend in higher temperatures, (ii) acetone with selectivity values ranging from 14% (400 °C) to 24% (750 °C), (iii) allyl alcohol with selectivity values ranging between 24 and 34% for the whole temperature range and (iv) acetaldehyde and acetic acid with selectivity values ranging from 15 and 9% (400 °C) to 22 and 20% (750 °C), respectively.

In the case of Ni-ATLS a redox mechanism over the available oxygen vacancies may be assumed. Water may be adsorb and activated as surface hydroxyls over such vacancies reducing ATLS surface as it is difficult to be activated on Ni species [3,4]. Thus, reduced ATLS may have an interaction with the dehydrogenation intermediate species from Ni to formation of CO<sub>2</sub> and H<sub>2</sub>, closing the redox cycle of ATLS in WGS. However another coexisting mechanism cannot be excluded explaining the dual path of glycerol reaction via acetol and propenal.

## CONCLUSIONS

Despite the low specific surface area of ATLS materials, Ni/ATLS catalysts presented an impressive performance in comparison with Ni-ALO catalysts in the GSR reaction. The larger Ni crystallites exhibit excellent low temperature conversion rates and selectivity towards H<sub>2</sub> production. Ni-ATLS superior performance can be attributed to the existence of a redox GSR mechanism which enables the mobility and storage of lattice oxygen, by enhancing WGS reaction to high H<sub>2</sub> yield. Further work is under development in order to clarify the correlation of the surface properties of the ATLS materials with the active catalyst towards the better understanding of the GSR mechanism.

## AKNOWLEDGEMENTS

Financial support by the programs THALIS and Archimedes III implemented within the framework of Education and Lifelong Learning Operational Programme, co-financed by the Hellenic Ministry of Education, Lifelong Learning and Religious Affairs and the European Social Fund, The authors wish also to acknowledge financial support provided by the Committee of the Special Account for Research Funds of the Technological Educational Institute of Western Macedonia (ELKE, TEIWM, Grant number: 80126).

## REFERENCES

1. A. Corma, G. Huber, L. Sauvanaud and P. Oconnor, *J. Catal.*, 2008, 257, 163–171.
2. N. H. Tran and G. S. Kannangara, *Chem. Soc. Rev.*, 2013, 42, 9454–9479.
3. K. N. Papageridis, G. Siakavelas, N. D. Charisiou, D. G. Avraam, L. Tzounis, K. Kousi and M. A. Goula, *Fuel Process. Technol.*, 2016, 152, 156–175.
4. S. Li and J. Gong, *Chem. Soc. Rev.*, 2014, 43, 7245–7256.
5. P. K. Pandis, E. Xenogiannopoulou, P. M. Sakkas, G. Sourkouni, C. Argiris and V. N. Stathopoulos, *RSC Adv.*, 2016, 6, 49429–49435.
6. T. Wakabayashi, S. Kato, Y. Nakahara, M. Ogasawara and S. Nakata, *Catal. Today*, 2011, 164, 575–579.
7. T. S. Kharlamova, A. S. Matveev, A. V. Ishchenko, A. N. Salanov, S. V. Koshcheev, A. I. Boronin and V. A. Sadykov, *Kinet. Catal.*, 2014, 55, 361–371.
8. M. A. Goula, N. D. Charisiou, P. K. Pandis and V. N. Stathopoulos, *RSC Adv.*, 2016, 6, 78954
9. H. Gasparyan, S. Neophytides, D. Niakolas, V. Stathopoulos, T. Kharlamova, V. Sadykov, O. Van der Biest, E. Jothinathan, E. Louradour, J. P. Joulin and S. Bebelis, *Solid State Ionics*, 2011, 192, 158–162.
10. V. Sadykov, E. Sadovskaya, A. Bobin, T. Kharlamova, N. Uvarov, A. Ulikhin, C. Argiris, G. Sourkouni and V. Stathopoulos, *Solid State Ionics*, 2015, 271, 69–72.